Direct Measurement of Charge Reversal on Lipid Bilayers using Heterodyne-Detected Second Harmonic Generation Spectroscopy

HanByul Chang, Paul E. Ohno, Yangdongling Liu, Emilie H. Lozier, Naomi Dalchand, and Franz M. Geiger*

Department of Chemistry, Northwestern University, 2145 Sheridan Road, Evanston, Illinois 60660, United States

ABSTRACT. We report the detection of charge reversal induced by the adsorption of a cationic polyelectrolyte, poly(allylamine) hydrochloride (PAH), to buried supported lipid bilayers (SLBs), used as idealized model biological membranes. Through the use of an α-quartz reference crystal, we quantify the total interfacial potential at the interface in absolute units, using HD-SHG as an optical voltmeter in which the traditional wire leads of a voltmeter have been replaced by photons. This quantification is made possible by isolating from other contributions to the total SHG response the phase-shifted potential-dependent third-order susceptibility. We detect the sign and magnitude of the surface potential and the point of charge reversal at buried interfaces without prior information or complementary data. Isolation of the second-order susceptibility contribution from the overall SHG response allows us to directly characterize the Stern and Diffuse Layers over single-component SLBs formed from three different zwitterionic lipids of different gel-to-fluid phase transition temperatures (T_ms). We determine whether the surface potential changes with the physical phase state (gel, transitioning, or fluid) of the SLB and incorporate 20 percent of negatively charged lipids to the zwitterionic SLB to investigate how the surface potential and the second-order nonlinear susceptibility $\chi^{(2)}$ change with surface charge.

*Corresponding author: geigerf@chem.northwestern.edu

I. Introduction. Charge reversal is an interfacial phenomenon characterized by the reversal of native surface charge through the adsorption of ions, occurring primarily in systems with high-valence ions, large surfactants, polyelectrolytes, and biological complexes.[1-11] A comprehensive understanding of charge reversal is needed to accurately predict and control electrostatic interactions at charged surfaces for applications in many fields ranging from materials science to environmental chemistry to microbiology. Factors leading to charge reversal are believed to include ion size asymmetry, the discontinuous dielectric constant of interfacial water, heterogeneity in the magnitude of the surface charge distribution, and salt concentrations.[2] Therefore, charge reversal is difficult to predict or explain using, for instance, mean field theory or Bragg-Williams approaches, given that they do not take into account non-Coulombic interactions and specific ion effects.[7,11,12] In this context, label-free techniques that directly probe interfacial charges and potentials under ambient conditions and in real time as they undergo charge reversal are needed.[13-15]

Here, we employ heterodyne-detected second harmonic generation (HD-SHG)[16,17] to directly detect charge reversal at a negatively charged, largely zwitterionic supported lipid bilayer, used here as an idealized model of a biological membrane,[18] upon adsorption of the cationic polyelectrolyte poly(allylamine) hydrochloride (PAH, 160mer). This commercially available polycation is used in various applications including gene therapy[19] and drug delivery.[20] Prior SHG and quartz crystal microbalance mass measurements showed the PAH surface coverage increases with [PAH] to full surface saturation,[21] while SFG spectroscopy indicated no membrane disruption under these conditions.[22,23] Now, we demonstrate the utility of HD-SHG for detecting both the sign of $\Phi(0)$ and the point of charge reversal at buried interfaces without any additional information or complementary techniques. Use of an α-quartz reference crystal in place of the

liquid water allows us to quantify the potential at the interface in absolute units, turning HD-SHG into an optical voltmeter in which the traditional wire leads of a voltmeter have been replaced by photons. Furthermore, isolation of the $\chi^{(2)}$ contribution from the overall SHG response allows us to directly monitor the Stern Layer such that the validity and applicability of atomistic simulations of aqueous:solid interfaces can be tested. Finally, we characterize the Stern and Diffuse Layers over single-component SLBs formed from three different zwitterionic lipids of different gel-to-fluid phase transition temperatures (T_ms). We determine whether the surface potential changes with the physical phase state (gel, transitioning, or fluid) of the SLB and incorporate 20 percent of negatively charged lipids to the zwitterionic SLB to investigate how the surface potential changes with surface charge.

II. Heterodyne-Detected Second Harmonic Generation Signals from Electrical Double Layers. HD-SHG is sensitive to the polarization of water molecules in the electrical double layer (EDL) that is set up by the static E-field produced by surface charges, enabling a direct determination of the interfacial potential, $\Phi(0)$. The structure and composition of the EDL and the magnitude of $\Phi(0)$ remain topics of theoretical and experimental interest, with mean-field models often used to describe the EDL.[24] One widely used model divides the EDL into the Stern and the Diffuse Layers.[25-28] The Stern Layer contains tightly adsorbed species (water, ions) near the dividing plane of the interface and has been recently referred to as a bonded interfacial layer.[29] In contrast, the Diffuse Layer is comprised of water molecules and ions farther away from the surface in the region where $\Phi(z)$ decays with distance, z, such that $\Phi(z=\infty) = 0$. While the potential is commonly assumed to decay exponentially, as predicted by Poisson-Boltzmann statistics,[2,11,12,30,31] other distance dependent expressions are possible as well, as will be discussed below.

As recently demonstrated,[16,17] HD-SHG allows us to separate the signals generated in the Stern and the Diffuse Layers through the independent determination of the SHG phase and amplitude, making the detection of the point of charge reversal straightforward and giving us insights into the process without any need for prior knowledge of the sign or magnitude of the interfacial charge density at the beginning of the experiment. Working far away from electronic or vibrational resonances allows us to treat the contributions to the SHG response as purely real. Indeed, nonresonant homodyne-detected SHG has been widely used in label-free *in situ* studies of charged surfaces.[32-35] Accounting for dispersion between the fundamental and second harmonic beams within the EDL, the interpretation of nonresonant SHG data from charged interfaces is based on the following model:[21,29,36-49]

$$E_{\mathrm{sig}}e^{i\varphi_{sig}} \propto \chi^{(2)} + \chi^{(3)}\Phi(0)\cdot T(\varphi_{DC})e^{i\varphi_{DC}} = \chi^{(2)'}_{eff,sample} \quad (1)$$

Here, E_{sig} and φ_{sig} represent the magnitude and phase of the SHG response, respectively, $\chi^{(2)}$ and $\chi^{(3)}$ are the second- and third-order nonlinear susceptibility tensors of the interfacial system, $\Phi(0)$ is the total interfacial potential, and $T(\varphi_{DC})e^{i\varphi_{DC}}$ represents the phase matching correction term as will be discussed below. As expressed in eqn. 1, we use the term $\chi^{(2)'}_{eff,sample}$ to characterize the total response of the interface, where the " $'$ " has been added to emphasize that the nominally second-order term includes both $\chi^{(2)}$ and $\chi^{(3)}$ contributions, as defined here. The total interfacial potential, $\Phi(0)$, is given by the sum of the electrostatic Coulomb potential and the potential due to net-aligned dipoles, i.e. the dipole potential: $\Phi_{total}(0) = \Phi_{Couloumb}(0) + \Phi_{dipole}(0)$. This latter potential is important for many uncharged (neutral, zwitterionic) interfacial systems and can be on the order of several 100 mV.[50]

Off-resonant HD-SHG provides all of the phase information required for separating $\chi^{(2)}$ from $\chi^{(3)}\Phi(0)$, while current versions of single-step HD-SFG only reference the phase in the absorptive elements of $\chi^{(2)}$. Use of Model (1) relies on three assumptions: a) the nonlinear optical signal recorded at the detector consists of only second- and third-order terms, b) the surface potential decays somehow with distance, and c) Debye-Hückel theory is applicable for the bulk aqueous phase, which is a reasonable assumption below ~0.1M ionic strength.

The $\chi^{(2)}$ and $\chi^{(3)}$ contributions are now understood[29,37,51-58] to originate in the Stern and Diffuse Layers, respectively. The second-order term, $\chi^{(2)}$, reports on the Stern Layer and is specific to the identity and polarization of molecules and ions in that region.[59,60] In contrast, the third-order $\chi^{(3)}$ term is of bulk origin[37] and originates from the water molecules and ions in the Diffuse Layer.[29,61,62] The phase shift of the $\chi^{(3)}$ term with respect to $\chi^{(2)}$ ("$e^{i\varphi_{DC}}$") results from the fact that at low ionic strength, the EDL becomes significantly long so that $\chi^{(3)}$ is generated at different EDL depths,[16,36] with optical dispersion causing a phase shift in the $\chi^{(3)}$ term. This phase shift, when measured in conjunction with the amplitude of the SHG signal, allows separation of the Stern and Diffuse Layers.[16,17]

The trigonometric function T(φ_{DC}) and the angle of the DC-field induced term, φ_{DC}, in eqn. 1 depend on the functional form of the variation of $\Phi(z)$ with distance, z, from the interface. For an exponentially decaying potential of the form $\Phi(z) \propto e^{-z\lambda_D^{-1}}$,[37] we find that $T = \cos(\varphi_{DC})$ and $\varphi_{DC} = \arctan(\Delta k_z\, \lambda_D)$,[16,48] where Δk_z is the wavevector mismatch of the optical process (1.07×10^7 m^{-1} in our case)[16] and λ_D is the Debye screening length in the bulk aqueous solution, which is readily estimated using Debye-Hückel theory. At high ionic strength, the Debye length is < 1 nm. Since $\varphi_{DC} \to 0$ in that limit, and since $\Phi(0) \to 0$, $\chi^{(2)}$ dominates the SHG response in

eqn. 1. At low ionic strength, $\Phi(0)$ is non-zero and the Debye length can be several hundred nm or longer. Then, $\varphi_{DC} \rightarrow \frac{\pi}{2}$ and optical interference in the Diffuse Layer is considerable and measurable through the $\chi^{(3)}$ contribution. We also consider the case of a linearly decaying potential[37] and find that the differences in the trigonometric factors for the linear and the exponential decays of $\Phi(z)$ are about 50% in the dilute limit (100 nm screening length). In the high ionic strength limit (1 nm screening length), the difference is smaller than 1%. Derivations can be found in Supporting Information, Section S1.

III. Experimental Methods

III.A. Preparation of Optical Cell and Substrate. Fused silica hemispheres (ISP Optics, QU-HS-25) were cleaned in NOCHROMIX (Godax Laboratories) cleaning solution for 1 hour and rinsed with ultrapure water. The hemispheres were then sonicated in methanol for 15 minutes, dried with N_2, air plasma cleaned for 15 minutes on the highest setting, and stored in ultrapure water until use. A custom-built PTFE cell was sonicated in methanol for 15 minutes, rinsed with ultrapure water, dried with N_2, then air plasma cleaned for 15 minutes prior to each experiment. The cell was then inserted into an aluminum exterior for added clamping rigidity to minimize movement of the hemisphere during experiments. A fluoroelastomer O-ring was placed between the interior cell and the hemispheres to ensure that the wetted part of the hemisphere is in contact only the fluoroelastomer and PTFE.

III.B. Solution and Vesicle Preparation. Trizma base buffer solutions were prepared in ultrapure water (18.2 MΩ cm^{-1}; MilliporeSigma) and pH-adjusted to pH 7.4 using small aliquots of diluted HCl and NaOH. PAH (Sigma Aldrich, 283215) solutions were made in 0.01 mM NaCl solution without further purification. Each of the pure water, salt, and PAH solutions containing no buffer were air-equilibrated overnight to ~ pH 5.5 ± 0.3. Dioleoyl-sn-glycero-3-phosphocholine (DOPC),

1,2-dimyristoyl-sn-glycero-3-phosphocholine (DMPC), and 1,2-distearoyl-sn-glycero-3-phosphocholine (DSPC) (10 mg mL^{-1} in chloroform) and 1,2-dimyristoyl-sn-glycero-3-phospho-(1'-rac-glycerol) (DMPG) (lyophilized powder) were purchased from Avanti. DMPG was dissolved into 25 mg mL^{-1} solution using neat chloroform (B&J Brand). The lipids were dried under gentle N_2 gas in glass vials and placed in a vacuum desiccator for at least 6 hours. The dried vesicles were then rehydrated in 1 mL 0.1 M NaCl, 10 mM Tris, 5 mM $CaCl_2$, pH 7.4 for at least 30 minutes. DSPC was hydrated and extruded at ~65 ˚C on a heating mantle (at least 10 ˚C above its transition temperature). Unilamellar lipid vesicles were prepared by extrusion though a 0.05 μm membrane filter (Avanti, 610000) thirteen times. The vesicles were diluted to 0.5 mg mL^{-1} with the hydrating buffer right before the formation of SLB. Chemical structures of lipids used in this work and PAH can be found in Figure 1.

III.C. Formation of SLBs and HD-SHG Spectroscopy. Following our previous work,[63] calcium-free 0.1 M NaCl, 10 mM Tris buffer (pH 7.4) solution was introduced into the flow cell first, and the SHG response was recorded until a steady signal was attained for at least 10 minutes. Next, 4 mL of diluted vesicles were introduced into the cell at 2 mL min^{-1} and allowed to self-assemble into a lipid bilayer on the silica substrate for at least 40 min using the vesicle fusion method.[64] Following bilayer formation, 20 mL of the 0.1 M NaCl, 10 mM Tris buffer solution at pH 7.4 was flushed through the cell to remove any excess vesicles, after which a 0.1 M NaCl solution air-equilibrated overnight (pH 5.8) was introduced until steady signal was recorded for at least 10 minutes. After a steady SHG intensity signal was obtained, three SHG interference patterns were recorded in series by moving a piece of α-quartz along an automated 10 cm translational stage (details about our HD-SHG spectrometer are described in our earlier work).[16] For each pattern, 20 equidistant positions along the translational stage were selected, each with 20 seconds of signal

acquisition. Each pattern took approximately 7 minutes for a total of ~20 min per triplicate pattern. Then, either PAH solution, low [salt], or pure deionized water, all air-equilibrated overnight, was introduced, followed by another triplicate interference pattern acquisition. The solutions were alternated between high [salt] and either low [salt] or PAH solution three times for each experiment. All [PAH]-dependent and [salt]-dependent SHG experiments were carried out under continuous flow at 2 mL min^{-1}.

III.D. Observables, Referencing, and Data Interpretation. In our implementation of HD-SHG (described in the SI, Section S2), a sinusoidal function is fit to interference patterns generated by modulating the phase between the sample signal and a local oscillator to obtain the SHG amplitude, $E_{\text{sig,}}$ and the SHG phase, φ_{sig}.[16,17] Argand diagrams (Fig. 2) are well suited to represent the change in the real and imaginary components of individual $\chi^{(2)}$ and $\chi^{(3)}$ contributions generated by φ_{DC} and changes in surface potential. At high salt concentration (0.1 M), φ_{DC} is close to zero (Fig. 2A). As both our fundamental and SHG wavelengths are nonresonant with respect to any vibrational or electronic transitions of our experimental system, $\chi^{(2)}$ and $\chi^{(3)}$ are purely real. Therefore, E_{sig} is situated along the real axis.

We set the measured φ_{sig} from the interference pattern at high [salt] (0.1 M NaCl) equal to 0º and effectively use it as the reference for the measurements with varying [NaCl] or [PAH]. At low [salt] (Fig. 2B), the $\chi^{(3)}\Phi(0)\cos(\varphi_{DC})$ vector is rotated by the non-negligible value of φ_{DC} away from the real axis such that the SHG response, E_{sig}, also rotates away from the real axis. The angle of rotation around the Argand diagram origin is reported by φ_{sig}. Charge reversal is readily observed with HD-SHG because a flip in the sign of $\Phi(0)$ reverses the direction of $\chi^{(3)}\Phi(0)\cos(\varphi_{DC})$, leading to a sign flip in φ_{sig} (Fig. 2C).

Using the E_{sig} and φ_{sig} at a given salt concentration relative to high salt concentration (0.1 M) and the calculated DC phase angle at that salt concentration (recall that $\varphi_{DC} = \arctan(\Delta k_z\, \lambda_D) = f([NaCl])$ for an exponentially decaying $\Phi(z)$), we rearrange eqn. 1 to yield (derived in the SI, Section S3):

$$\Phi(0) \propto E_{sig} \frac{\sin(\varphi_{sig})}{\chi^{(3)} \cos(\varphi_{DC}) \sin(\varphi_{DC})} \tag{2a}$$

$$\chi^{(2)} \propto E_{sig} \left(\cos(\varphi_{sig}) - \sin(\varphi_{sig}) \frac{\cos(\varphi_{DC})}{\sin(\varphi_{DC})} \right) \tag{2b}$$

Here, E_{sig} and φ_{sig} are determined from a triplicate set of interference fringes recorded at a given salt concentration, and φ_{DC} is computed for that given ionic strength. Experiments[17,29,65] and computations[66] show that $\chi^{(3)}$ for water is invariant with the chemical composition and charge state of the interface and constant across a wide range of bulk pH and ionic strength. Thus, eqn. 2 yields $\Phi(0)$, which governs the energetics of interactions between charged species and the surface, and $\chi^{(2)}$, which gives information on surface chemistry or specific binding, from the measured E_{sig} and φ_{sig} at a given screening length in the bulk ionic solution.

III.E. Absolute Measurements of Φ(0) and $\chi^{(2)}$ through α-Quartz Referencing. Eqn. 2 allows the calculation, in arbitrary units, of values that are proportional to $\Phi(0)$ and $\chi^{(2)}$. While useful for investigating relative changes in these two parameters, ideally one desires their quantification in absolute units. Such an absolute quantification can be achieved through comparison of the sample signal with that of a reference with known nonlinear susceptibility, as shown in the following equation (derived in the SI, Section S4):

$$\Phi(0) = \left(\frac{E_{sig,sample}}{E_{sig,quartz}} \frac{F_{quartz}}{F_{sample}} \left| \chi^{(2)}_{eff,quartz} \right| \right) \frac{\sin(\varphi_{sig})}{\chi^{(3)} \cos(\varphi_{DC}) \sin(\varphi_{DC})} \tag{3a}$$

$$\chi^{(2)} = \left(\frac{E_{sig,sample}}{E_{sig,quartz}}\frac{F_{quartz}}{F_{sample}}\left|\chi^{(2)}_{eff,quartz}\right|\right)\left(\cos(\varphi_{sig}) - \sin(\varphi_{sig})\frac{\cos(\varphi_{DC})}{\sin(\varphi_{DC})}\right) \qquad (3b)$$

$E_{sig,sample}$ is measured for the sample surface of interest, $E_{sig,quartz}$ is measured for an α-quartz crystal in place of the sample surface, F_{quartz} and F_{sample} represent the macroscopic Fresnel coefficients (calculated in the SI, Section S5), and $\chi^{(2)}_{eff,quartz}$ is known (*vide infra*). Importantly, the proportionality from eqn. 2 has been replaced by an equal sign. By measuring the ratio $\frac{E_{sig,sample}}{E_{sig,quartz}}$ at one specific sample condition and calculating the value of $\Phi(0)$ and $\chi^{(2)}$ at this condition using eqn. 3, the entire data set calculated from eqn. 2 can be referenced to that condition, giving it absolute units. We performed this "quartz referencing procedure" using the condition of 0.01 mM NaCl at pH 5.8 with no PAH added (the bare bilayer at low ionic strength).[67] The ratio $\frac{E_{sig,sample}}{E_{sig,quartz}}$ was obtained in homodyne detection mode (i.e. direct direction of the sample and quartz reference signals with the detector, with no local oscillator) using 7 mW of incident laser power from the same laser as the HD-SHG experiments.

First, a bilayer was formed from a 9:1 mix of DMPC:DMPG as described above. After flushing with buffer solution for 10 minutes, the buffer was replaced with a 0.1 M NaCl solution (air equilibrated over night to pH 5.8) until the SHG signal intensity was at steady state for at least 10 minutes. The salt solution was then replaced with a 0.01 mM NaCl solution and the SHG signal intensity was recorded until it reached steady state for ten minutes under continuous aqueous flow. This SHG intensity was then noted in terms of number of SHG counts per second, and $E_{sig,quartz}$ calculated from its square root. Then, the fused silica hemisphere was removed from the cell and replaced by a fused silica hemisphere to which a rectangular piece of z-cut α-quartz (10 mm x 5 mm x 3 mm, Knight Optical) was attached directly onto the flat side using a refractive index

matching optical adhesive (Norland, 146H). In preparation, the rectangular z-cut α-quartz crystal and the hemisphere were cleaned by sonicating in methanol for 6 minutes, followed by sonication in water for 6 minutes. Both were put in an oven for 1 minute and subsequently plasma cleaned for 1 more minute. The crystal was oriented with the x-axis parallel to the plane of incidence (the orientation of maximum intensity in S_{in}, P_{out}). As with the bilayer, the SHG signal intensity from the fused silica:α-quartz interface was recorded for at least 10 minutes to ensure there were no drifts in the signal intensity. Then, we computed the square root of the SHG signal intensity measured from our fused silica:α-quartz interface to obtain $E_{sig,quartz}$. The ratio $\frac{E_{sig,sample}}{E_{sig,quartz}}$ was found to equal (1/(37 ± 12), from 2 replicates, each performed on 2 separate days).

The value $\left|\chi^{(2)}_{eff,quartz}\right|$ is vastly dominated by the bulk response of α-quartz ($\chi^{(2)}_{Bulk,Q} = 8 \times 10^{-13}$ mV^{-1}),[68,69] and we calculate $\left|\chi^{(2)}_{eff,quartz}\right| = 4.5 \times 10^{-20}$ m^{2}V^{-1} in our experimental geometry, as shown in the SI, Section S5. Finally, we use the experimentally determined value of $\chi^{(3)} = -(9.6 \pm 1.9) \times 10^{-22}$ m^{2}V^{-2} recently reported for off-resonant SHG by Wen and coworkers[67] (*n.b.*, an earlier model using experimental and quantum mechanical inputs yields $\chi^{(3)} = -10.3 \times 10^{-22}$ m^{2}V^{-2}).[70] We then have all the parts needed to obtain $\chi^{(2)}$ and $\Phi(0)$, in absolute units, from eqn. 3.

IV. Results and Discussion.

IV.A. Direct Measurement of Charge Reversal and Resulting Change in $\Phi(0)$. We first investigate the adsorption of the cationic PAH onto a negatively charged bilayer formed from a 9:1 mix of DMPC:DMPG. The experiments are carried out with 0.01 mM NaCl background solution to minimize the relative change in ionic strength with the addition of the highest PAH concentration, 10 nM (0.0032 mM ionic strength from the 160 charged units on PAH and 160

counter ions) while staying within the low ionic strength regime where φ_{sig} can be measured readily. We nevertheless account for the small change in ionic strength with increasing [PAH] when computing φ_{DC}, which changes by <10%, only negligibly impacting the final $\Phi(0)$ values compared to unadjusted values. The values with and without the additional ionic strength correction are presented in the Supporting Information, Section S6.

Fig. 3A shows that the introduction of 1 nM PAH in 0.01 mM NaCl lowers φ_{sig} when compared to that recorded for the PAH-free 0.01 mM NaCl over the bilayer when referenced to condition of 0.1 M NaCl at the same pH. However, the sign of the measured phase angle is still positive. Likewise, E_{sig} (normalized to E_{sig} at 0.01 mM NaCl) decreases. Given that the DC phase angle, φ_{DC}, does not change under the conditions of controlled ionic strength, and given that $\chi^{(3)}$ is constant,[24] the observations are consistent with a decrease in the magnitude of the surface potential, $\Phi(0)$, that is expected upon adsorption of a polycation to a negatively charged surface. With increasing PAH concentrations, φ_{sig} and E_{sig} decrease further, with φ_{sig} crossing the 0º mark at ~4 nM, signaling the point of charge reversal, after which φ_{sig} has changed sign and continues to increase in the negative direction.

Using eqn. 2, we now obtain $\Phi(0)$ and $\chi^{(2)}$ from the observables φ_{sig} and E_{sig}, again assuming an exponentially decaying potential. Following the discussion above, we use eqn. 3 to reference both axes to the condition at 0.01 mM NaCl and assign absolute units. The absolute value of $\chi^{(2)}$ at 0.01 mM NaCl and pH 5.8 for the 9:1 DMPC:DMPG bilayer is $1.3 \pm 0.5 \times 10^{-22}$ m^2 V, which is in good agreement with experimental reports for DOPC liposomes albeit with a greater error,[71] and agrees with computational estimates[72] as well as nonresonant SFG responses from a variety of non-absorbing liquids in contact with air.[73] The values are also in good agreement with

those reported more recently by Dalstein et al.[65] who reported $\chi^{(2)}$ values for lignoceric acid monolayer:water interfaces using non-resonant SHG measurements.

Fig. 3B shows that PAH adsorption coincides with a change in surface potential from -0.18 ± 0.08 V before PAH addition to +0.03 ± 0.01 V at saturation, presumably through polycation adsorption to the negatively charged surface and a corresponding lowering of the interfacial charge density until the point of charge reversal, when $\Phi(0)$ reverses its sign as PAH adsorption continues (*n.b.* PAH surface coverages and free energies of adsorption obtained by our earlier homodyne-detected SHG experiments coupled to quartz crystal microbalance measurements are considerable under our experimental conditions.)[21] At this point, $\Phi(0)$ is ~ 15% of what it was without added PAH, and, again, oppositely signed.

Unlike earlier studies reporting that $\chi^{(2)}$ flips sign at mineral:water interfaces when adjusting the bulk solution pH from above to below the point of zero charge,[74] or at air:lipid monolayer:water interfaces with oppositely charged lipids,[75] $\chi^{(2)}$ remains positively-valued in our case while not changing much in magnitude. Upon PAH-induced charge reversal, the number density of attached PAH is substantial, with direct contact ion pair formation between the lipid headgroups and the ammonium groups of the PAH,[76] such that now $\chi^{(2)}_{total} = \chi^{(2)}_{Silica} + \chi^{(2)}_{bilayer} + \chi^{(2)}_{PAH} + \chi^{(2)}_{water} + \chi^{(2)}_{ions}$ ($\chi^{(2)}_{water}$ in this equation refers to the tightly bound water molecules right at the interface, rather than in the Diffuse Layer).[29] In terms of polarization charge density, the largest contributor to the SHG response is expected to be the lipid bilayer. While lipids can readily flip,[77-84] the sign of $\chi^{(2)}_{bilayer}$ would not change as the number of lipids pointing up and down to form the bilayer is approximately constant for these similarly sized lipids.

The relatively modest change, if any, in $\chi^{(2)}$ seen in Fig. 3B further confirms that the change in E_{sig} is dominated by the change in the potential-dependent $\chi^{(3)}$ term. Given that $\chi^{(2)}$ is comprised of constructive (in-phase) and destructive (out-of-phase) contributions from the silica, the lipid bilayer, the water molecules, the ions, and PAH, any net change in $\chi^{(2)}$ is likely to be due to a combination of a loss of water molecules (as we recently reported using vibrational sum frequency generation spectroscopy)[39] and thus a reduction in $\chi^{(2)}_{water}$ on the one hand and a gain in $\chi^{(2)}_{PAH}$ due to PAH adsorption on the other.

There are two determinants of Φ(0): the charge density, σ(0), and the ionic strength of the aqueous solution. The former can be described by mean field models, e.g. the Gouy-Chapman model, which works well up to moderate charge densities. Our previously published work shows that σ(0) at the lipid membrane:water interfaces is −0.024 (+0.003/−0.005) C/m^2 at pH 7.[85] This value is below what has been reported to lead to breakdowns of Gouy-Chapman theory for describing charged Langmuir monolayers (>0.3 Cm^{-2}).[86] If we then compute the surface potential using the Gouy-Chapman model according to $\Phi(0) = \frac{2k_BT}{ze}\sinh^{-1}\frac{\sigma}{\sqrt{8000k_BTN_AC_{elec}\varepsilon_0\varepsilon_R}}$, where k_B is the Boltzman constant, z is the charge of the electrolyte, e is the fundamental charge of an electron, $C_{elec}$is the concentration of the electrolyte, ε_0 is the relative permittivity of vacuum, ε_R is the relative permittivity of bulk water at 25 ˚C, and σ is the surface charge density, we find sizeable surface potentials at the low ionic strengths employed here, $\Phi(0) = -0.25$ V at the low ionic strength used in this work (0.01 mM), in agreement with the -0.18 (± 0.08) V total surface potential obtained in the experiment.

As a final note regarding the determination of the sign of the potential and charge reversal, the direction of the phase shift does not change when the reference quartz crystal is rotated by 60°

although we can observe the expected 180° phase shift (SI, Section S7), providing an additional practical advantage that the absolute orientation of the quartz crystal does not have to be known to determine the sign of the surface potential.

III.B. $\chi^{(2)}$ and $\Phi(0)$ do not Change with Bilayer Fluidity but with Membrane Surface Charge. As an additional demonstration of the utility of HD-SHG for studying lipid bilayer membranes, we investigated three different, previously characterized,[87] zwitterionic SLBs with different gel-to-fluid transition temperatures, T_m. We specifically used bilayers formed from pure (zwitterionic) DOPC, DMPC, and DSPC, each in the fluid, transitioning, and gel phase, respectively, as well as a bilayer formed from an 8:2 mix of (zwitterionic) DMPC and (negatively charged) DMPG that we had previously characterized as well.[88] Hysteresis effects that are important for the fused silica:water system under some conditions[16,58,89] were investigated here as well by introducing pure water followed by 0.1 M NaCl (instead of 0.1 M NaCl first) and no difference in φ_{sig} or normalized E_{sig} was observed between the two sequences, as described in Supporting Information, Section S8.

As described in the methods section, φ_{sig} is determined by subtracting φ_{fit} obtained for the condition of pure water from φ_{fit} at the condition of 0.1 M NaCl above a given bilayer. The E_{sig} point estimate that is initially normalized to the condition of 0.1m M NaCl for each bilayer is now further normalized to the normalized E_{sig} at 0.01 mM NaCl over 9:1 DMPC:DMPG in order to perform similar analyses for absolute quantification of $\Phi(0)$ as described in the previous section. We note that, in this analysis, we assume that the optical response of each bilayer at 100 mM NaCl is the same across bilayers and is dominated by the $\chi^{(2)}$ term.

Fig. 4A shows that there are no significant differences in φ_{sig} (~ 15˚) or the normalized E_{sig} for the pure bilayers, while the corresponding values for the bilayers formed from the 9:1 and the 8:2 zwitterionic:negatively charged lipid mixes are statistically significantly different. The same

outcome is obtained for the $\chi^{(2)}$ and $\Phi(0)$ values of the pure zwitterionic bilayers (Fig. 4B), consistent with the fact that the polarization charge density (number of electrons per lipid) and $\Phi(0)$ vary little when going from DOPC to DMPC to DSPC at constant ionic strength.

Because of the underlying assumption about $\chi^{(2)}$ as stated earlier, $\chi^{(2)}$ probed here is a poor indicator of the physical phase state (gel vs. fluid) of the SLBs we surveyed. However, when ten or 20 percent negatively charged DMPG is mixed in with zwitterionic DMPC, the $\Phi(0)$ point estimates increase towards more negative values, as would be expected due to the addition to negative charge while holding the ionic strength constant (from – 0.09 ± 0.04 V (DMPC) to -0.18 ± 0.07 V (10 percent DMPG) and to -0.22 ± 0.09 V (20 percent DMPG)). Yet, we caution that the uncertainties due to error propagation need to be lowered to make any further statements.

IV. Conclusion Heterodyne-detected second harmonic generation (HD-SHG) presents considerable advantages over homodyne detection by enabling separations of the various contributions to the total SHG signal. We unambiguously determine the sign of the potential as well as the point of charge reversal of supported lipid bilayers interacting with a common polycation by observing the reversal in the sign of the phase angle. HD-SHG can now be used in fundamental explorations for charge reversal of a wide range of buried interfaces and their interactions without prior knowledge or intuition regarding the interfacial electrostatics. Additionally, HD-SHG requires only one phase measurement at one aqueous phase condition of pH, ionic strength, or analyte concentration, thereby dramatically speeding up the process of determining the interfacial potential when compared to prior (homodyne-detected) approaches.

We also provide quantitative properties of the EDL of three lipid bilayers of varying T_ms of the same charge as well as an SLB with a more negative charge. We find that the phase angles of the three zwitterionic SLBs do not differ significantly and conclude that the fluidity of the SLB

does not change the structure of the EDL as long as the surface charge remains comparable. This observation is in support of the notion that EDL properties in the systems studied here are mainly governed by the DC-field induced by surface charge. Since the zwitterionic lipids surveyed here have comparable surface charge densities, we do not expect the potential associated with the EDL to change significantly. The addition of negatively charged DMPG lipid to the zwitterionic DMPC bilayer leads to increased $\Phi(0)$ point estimates, consistent with an increased surface potential originating from the increased surface charge. Furthermore, absolute quantification of $\chi^{(2)}$ and $\Phi(0)$ of the 9:1 DMPC:DMPG bilayer at each PAH concentration is achieved by comparing the extracted value from HD-SHG to an external α-quartz reference of known nonlinear susceptibility.

Combining the capability of HD-SHG to separate individual nonlinear susceptibilities and the visualization of the process enabled by Argand diagram, we are no longer restricted to studying only charged surfaces and particles. Interactions with uncharged (neutral) surfaces can be investigated by resonant HD-SHG, which molecularly specific. In resonant SHG experiments, the $\chi^{(2)}$ contribution is comprised of resonant ($\chi^{(2),R}$) and non-resonant ($\chi^{(2),NR}$), with $\chi^{(2),R}$ dominating the SHG signal.[90-103] Since $\chi^{(2),R}$ is directly related to the number of surface species in resonance with the fundamental and/or SH wavelength,[104] we can envision conducting HD-SHG experiments as a function of surface coverage of the resonant (as opposed to non-resonant species, like the PAH studied here) species. In this case, the phase shift between the two $\chi^{(2)}$ contributions is 90°; hence, $\chi^{(2),R}$ is represented by an additional vector perpendicular to the $\chi^{(2),NR}$ ($\chi^{(2)}$ in the current Argand plot).[90] Because the earlier homodyne-detected resonant SHG experiments do not measure phase, they were carried out under the assumption and requirement that the signal is dominated by the resonant species. The two tool discussed here circumvents the need for these limitations. Since HD-SHG can discriminate coherent SHG light from light generated at the second harmonic

wavelength from other optical processes as only coherent SHG light will interfere with the LO,[16] one can now operate even in a regime where fluorescence is present.

V. Associated Content

Supporting Information: Derivations of linearly decaying potential model equations; Fresnel coefficients; detailed derivation of eqn. 3; sample calculations using eqn. 3; and control experiments and hysteresis experiments.

VI. Author Information

Corresponding Author: geigerf@chem.northwestern.edu

ORCID:

HanByul Chang: 0000-0003-0270-7336

Paul E. Ohno: 0000-0003-4192-1888

Yangdongling Liu: 0000-0003-2750-9360

Franz M. Geiger: 0000-0001-8569-4045

VII. Acknowledgement. This work is supported by the National Science Foundation under the Center for Sustainable Nanotechnology, Grant No.CHE-1503408. This work was also supported by the US National Science Foundation (NSF) under its graduate fellowship research program (GRFP) award to PEO. PEO also acknowledges support from the Northwestern University Presidential Fellowship. FMG acknowledges support from a Dow Chemical Company Professorship and from the Alexander von Humboldt Foundation.

References.

(1) Rochín-Wong, S.; Rosas-Durazo, A.; Zavala-Rivera, P.; Maldonado, A.; Martínez-Barbosa, M. E.; Vélaz, I.; Tánori, J.; "Drug Release Properties of Diflunisal from Layer-By-Layer Self-Assembled κ-Carrageenan/Chitosan Nanocapsules: Effect of Deposited Layers" *Polymers (Basel)* **2018**, *10*, 760.

(2) Wang, Z.-Y.; Zhang, P.; Ma, Z.; "On the physics of both surface overcharging and charge reversal at heterophase interfaces" *Physical Chemistry Chemical Physics* **2018**, *20*, 4118.

(3) Richardson, J. J.; Tardy, B. L.; Ejima, H.; Guo, J.; Cui, J.; Liang, K.; Choi, G. H.; Yoo, P. J.; De Geest, B. G.; Caruso, F.; "Thermally Induced Charge Reversal of Layer-by-Layer Assembled Single-Component Polymer Films" *ACS Applied Materials & Interfaces* **2016**, *8*, 7449.

(4) Liu, X.; Xiang, J.; Zhu, D.; Jiang, L.; Zhou, Z. P.; Tang, J.; Liu, X.; Huang, Y.; Shen, Y.; "Fusogenic Reactive Oxygen Species Triggered Charge-Reversal Vector for Effective Gene Delivery" *Adv. Mat.* **2016**, *28*.

(5) Yuan, Y. Y.; Mao, Q. C.; Du, X. J.; Du, J. Z.; Wang, F.; Wang, J.; "Surface Charge Switchable Nanoparticles Based on Zwitterionic Polymer for Enhanced Drug Delivery to Tumor" *Adv. Mat.* **2012**, *24*.

(6) Becraft, K. A.; Moore, F. G.; Richmond, G. L.; "Charge Reversal Behavior at the CaF2/H2O/SDS Interface as Studied by Vibrational Sum Frequency Spectroscopy" *J. Phys. Chem. B* **2003**, *107*, 3675.

(7) Cuvillier, N.; Rondelez, F.; "Breakdown of the Poisson-Boltzmann description for electrical double layers involving large multivalent ions" *Thin Solid Films* **1998**, *327-329*, 19.

(8) Decher, G.; "Fuzzy Nanoassemblies: Toward Layered Polymeric Multicomposites" *Science* **1997**, *277*, 1232.

(9) Rädler, J. O.; Koltover, I.; Salditt, T.; Safinya, C. R.; "Structure of DNA-Cationic Liposome Complexes: DNA Intercalation in Multilamellar Membranes in Distinct Interhelical Packing Regimes" *Science* **1997**, *275*, 810.

(10) Afshar-rad, T.; Bailey, A. I.; Luckham, P. F.; Macnaughtan, W.; Chapman, D.; "Forces between poly-l-lysine of molecular weight range 4,000–75,000 adsorbed on mica surfaces" *Colloids and Surfaces* **1987**, *25*, 263.

(11) Lyklema, J.; "Overcharging, charge reversal: Chemistry or physics?" *Colloids and Surfaces A: Physicochemical and Engineering Aspects* **2006**, *291*, 3.

(12) Jiménez-Ángeles, F.; Lozada-Cassou, M.; "A Model Macroion Solution Next to a Charged Wall: Overcharging, Charge Reversal, and Charge Inversion by Macroions" *The Journal of Physical Chemistry B* **2004**, *108*, 7286.

(13) Zaera, F.; "Probing Liquid/Solid Interfaces at the Molecular Level" *Chem. Rev.* **2012**, *112*, 2920.

(14) Björneholm, O.; Hansen, M. H.; Hodgson, A.; Liu, L.-M.; Limmer, D. T.; Michaelides, A.; Pedevilla, P.; Rossmeisl, J.; Shen, H.; Tocci, G.; Tyrode, E.; Walz, M.-M.; Werner, J.; Bluhm, H.; "Water at Interfaces" *Chem. Rev.* **2016**, *116*, 7698.

(15) Zaera, F.; "Surface chemistry at the liquid/solid interface" *Surface Science* **2011**, *605*, 1141.

(16) Ohno, P. E.; Chang, H.; Spencer, A. P.; Boamah, M. D.; Liu, Y.; Wang, H.-f.; Geiger, F. M.; "Beyond the Gouy-Chapman Model with Heterodyne-Detected Second Harmonic Generation" *chemRxiv* **2019**.

(17) Boamah, M. D.; Ohno, P. E.; Lozier, E.; Van Ardenne, J.; Geiger, F. M.; "Specifics about Specific Ion Adsorption from Heterodyne-Detected Second Harmonic Generation" *arXiv:1905.04148 and J. Phys. Chem. B* **2019**, *123*.

(18) Chan, Y. H. M.; Boxer, S. G.; "Model membrane systems and their applications" *Current Opinion in Chemical Biology* **2007**, *11*, 581.

(19) Antipov, A. A.; Sukhorukov, G. B.; Donath, E.; Möhwald, H.; "Sustained Release Properties of Polyelectrolyte Multilayer Capsules" *The Journal of Physical Chemistry B* **2001**, *105*, 2281.

(20) Vinogradova, O. I.; Lebedeva, O. V.; Vasilev, K.; Gong, H.; Garcia-Turiel, J.; Kim, B.-S.; "Multilayer DNA/Poly(allylamine hydrochloride) Microcapsules: Assembly and Mechanical Properties" *Biomacromolecules* **2005**, *6*, 1495.

(21) McGeachy, A. C.; Dalchand, N.; Caudill, E. R.; Li, T.; Dogangun, M.; Olenick, L.; Chang, H.; Pedersen, J. A.; Geiger, F.; "Interfacial Electrostatics of Poly(vinylamine hydrochloride), Poly(diallyldimethylammonium chloride), Poly-L-lysine, and Poly-L-arginine Interacting with Lipid Bilayers" *Physical Chemistry Chemical Physics* **2018**, *20*, 10846.

(22) Dalchand, N.; Dogangun, M.; Ohno, P. E.; Ma, E.; Martinson, A.; Geiger, F. M.; "Perturbation of Hydrogen Bonding Networks over Supported Lipid Bilayers by Poly (Allylamine Hydrochloride)" *10.26434/chemrxiv.7851503.v1* **2019**.

(23) Olenick, L. L.; Troiano, J. M.; Vartanian, A.; Melby, E. S.; Mensch, A. C.; Zhang, L.; Hong, J.; Mesele, O.; Qiu, T.; Bozich, J.; Lohse, S.; Zhang, X.; Kuech, T. R.; Millevolte, A.; Gunsolus, I.; McGeachy, A. C.; Doğangün, M.; Li, T.; Hu, D.; Walter, S. R.; Mohaimani, A.; Schmoldt, A.; Torelli, M. D.; Hurley, K. R.; Dalluge, J.; Chong, G.; Feng, Z. V.; Haynes, C. L.; Hamers, R. J.; Pedersen, J. A.; Cui, Q.; Hernandez, R.; Klaper, R.; Orr, G.; Murphy, C. J.; Geiger,

F. M.; "Lipid Corona Formation from Nanoparticle Interactions with Bilayers" *Chem* **2018**, *4*, 2709.

(24) Hiemenz, P. C.; Rajagopalan, R. *Principles of colloid and surface chemistry*; Taylor & Francis: Boca Raton, 1997.

(25) Langmuir, D. *Aqueous Environmental Chemistry*; Prentice Hall: Upper Saddle River, NJ 1997.

(26) Lyklema, J. *Fundamentals of Interface and Colloid Science*; Elsevier, 2000.

(27) Darlington, A. M.; Jarisz, T. A.; DeWalt-Kerian, E. L.; Roy, S.; Kim, S. H.; Azam, M. S.; Hore, D. K.; Gibbs, J. M.; "Separating the pH-Dependent Behavior of Water in the Stern and Diffuse Layers with Varying Salt Concentration" *J. Phys. Chem. C* **2017**, *121*, 20229.

(28) Brown, M. A.; Goel, A.; Abbas, Z.; "Effect of Electrolyte Concentration on the Stern Layer Thickness at a Charged Interface" *Angew. Chem. Int. Ed.* **2016**, *55*, 3790.

(29) Wen, Y.-C.; Zha, S.; Liu, X.; Yang, S.; Guo, P.; Shi, G.; Fang, H.; Shen, Y. R.; Tian, C.; "Unveiling Microscopic Structures of Charged Water Interfaces by Surface-Specific Vibrational Spectroscopy" *Phys. Rev. Let.* **2016**, *116*, 016101.

(30) Wang, Z.-y.; Ma, Y.-q.; "Monte Carlo determination of mixed electrolytes next to a planar dielectric interface with different surface charge distributions" *The Journal of Chemical Physics* **2009**, *131*, 244715.

(31) Guerrero-García, G. I.; González-Tovar, E.; Chávez-Páez, M.; Lozada-Cassou, M.; "Overcharging and charge reversal in the electrical double layer around the point of zero charge" *The Journal of Chemical Physics* **2010**, *132*, 054903.

(32) Ong, S.; Zhao, X.; Eisenthal, K. B.; "Polarization of water molecules at a charged interface; second harmonic studies of the silica/water interface" *Chem. Phys. Lett.* **1992**, *191*, 327.

(33) Eisenthal, K. B.; "Liquid interfaces probed by second-harmonic and sum-frequency spectroscopy" *Chem. Rev.* **1996**, *96*, 1343.

(34) Geiger, F. M.; "Second Harmonic Generation, Sum Frequency Generation, and χ(3): Dissecting Environmental Interfaces with a Nonlinear Optical Swiss Army Knife" *Annu. Rev. Phys. Chem.* **2009**, *60*, 61.

(35) Hayes, P. L.; Malin, J. N.; Jordan, D. S.; Geiger, F. M.; "Get charged up: Nonlinear optical voltammetry for quantifying the thermodynamics and electrostatics of metal cations at aqueous/oxide interfaces" *Chem. Phys. Lett.* **2010**, *499*, 183.

(36) Gonella, G.; Lütgebaucks, C.; de Beer, A. G. F.; Roke, S.; "Second Harmonic and Sum Frequency Generation from Aqueous Interfaces is Modulated by Interference" *J. Phys. Chem. C* **2016**, *120*, 9165.

(37) Ohno, P. E.; Saslow, S. A.; Wang, H.-f.; Geiger, F. M.; Eisenthal, K. B.; "Phase-referenced Nonlinear Spectroscopy of the alpha-Quartz/Water Interface" *Nature communications* **2016**, *7*, 13587.

(38) Schaefer, J.; Gonella, G.; Bonn, M.; Backus, E. H. G.; "Surface-specific vibrational spectroscopy of the water/silica interface: screening and interference" *Phys. Chem. Chem. Phys.* **2017**, *19*, 16875.

(39) Dalchand, N.; Doğangün, M.; Ohno, P. E.; Ma, E.; Martinson, A. B. F.; Geiger, F. M.; "Perturbation of Hydrogen-Bonding Networks over Supported Lipid Bilayers by Poly(allylamine hydrochloride)" *The Journal of Physical Chemistry B* **2019**, *123*, 4251.

(40) Reddy, S. K.; Thiraux, R.; Wellen Rudd, B. A.; Lin, L.; Adel, T.; Joutsuka, T.; Geiger, F. M.; Allen, H. C.; Morita, A.; Paesani, F.; "Bulk Contributions Modulate the Sum-Frequency Generation Spectra of Water on Model Sea-Spray Aerosols" *Chem* **2018**, *4*, 1629.

(41) Ohno, P. E.; Wang, H.-f.; Paesani, F.; Skinner, J. L.; Geiger, F. M.; "Second-Order Vibrational Lineshapes from the Air/Water Interface" *The Journal of Physical Chemistry A* **2018**, *122*, 4457.

(42) McGeachy, A. C.; Caudill, E. R.; Liang, D.; Cui, Q.; Pedersen, J. A.; Geiger, Franz M.; "Counting charges on membrane-bound peptides" *Chem. Sci.* **2018**, *9*, 4285.

(43) Doğangün, M.; Ohno, P. E.; Liang, D.; McGeachy, A. C.; Bé, A. G.; Dalchand, N.; Li, T.; Cui, Q.; Geiger, F. M.; "Hydrogen-Bond Networks near Supported Lipid Bilayers from Vibrational Sum Frequency Generation Experiments and Atomistic Simulations" *The Journal of Physical Chemistry B* **2018**, *122*, 4870.

(44) Boamah, M. D.; Ohno, P. E.; Geiger, F. M.; Eisenthal, K. B.; "Relative permittivity in the electrical double layer from nonlinear optics" *J. Chem. Phys.* **2018**, *148*, 222808.

(45) Ohno, P. E.; Wang, H.-f.; Geiger, F. M.; "Second-order spectral lineshapes from charged interfaces" *Nat. Commun.* **2017**, *8*, 1032.

(46) Pezzotti, S.; Galimberti, D. R.; Shen, Y. R.; Gaigeot, M.-P.; "Structural definition of the BIL and DL: a new universal methodology to rationalize non-linear $\chi(2)(\omega)$ SFG signals at charged interfaces, including $\chi(3)(\omega)$ contributions" *Phys. Chem. Chem. Phys.* **2018**, *20*, 5190.

(47) Pezzotti, S.; Galimberti, D. R.; Shen, Y. R.; Gaigeot, M.-P.; "What the Diffuse Layer (DL) Reveals in Non-Linear SFG Spectroscopy" *Minerals* **2018**, *8*, 305.

(48) Boamah, M. D.; Ohno, P. E.; Lozier, E.; van Ardenne, J.; Geiger, F. M.; "Specifics About Specific Ion Adsorption from Heterodyne-Detected Second Harmonic Generation" **2019**, *ChemRxiv.Preprint*.

(49) Hore, D. K.; Tyrode, E. C.; "Probing Charged Aqueous Interfaces Near Critical Angles: Effect of Varying Coherence Length" *The Journal of Physical Chemistry C* **2019**.

(50) Casper, C. B.; Verreault, D.; Adams, E. M.; Hua, W.; Allen, H. C.; "Surface Potential of DPPC Monolayers on Concentrated Aqueous Salt Solutions" *Journal of Physical Chemistry B* **2016**, *120*, 2043.

(51) Gonella, G.; Lutgebaucks, C.; de Beer, A. G. F.; Roke, S.; "Second Harmonic and Sum-Frequency Generation from Aqueous Interfaces is Modulated by Interference" *J. Phys. Chem. C* **2016**, *120*, 9165.

(52) Wang, H.-f.; "Sum frequency generation vibrational spectroscopy (SFG-VS) for complex molecular surfaces and interfaces: Spectral lineshape measurement and analysis plus some controversial issues" *Progress in Surface Science* **2016**, *91*, 155.

(53) Ohno, P. E.; Wang, H.-f.; Geiger, F. M.; "Second-Order Spectral Lineshapes from Charged Interfaces" *Nature communications* **2017**, *8*, 1032.

(54) Ohno, P. E.; Wang, H. F.; Paesani, F.; Skinner, J. L.; Geiger, F. M.; "Second-Order Vibrational Lineshapes from the Air/Water Interface " *J. Phys. Chem A* **2018**, *122*, 4457.

(55) Boamah, M. D.; Ohno, P. E.; Geiger, F. M.; Eisenthal, K. B.; "Relative Permittivity in the Electrical Double Layer from Nonlinear Optics" *J. Chem. Phys.* **2018**, *148*, 222808.

(56) Joutsuka, T.; Hirano, T.; Sprik, M.; Morita, A.; "Effect of Third-Order Susceptibility in Sum Frequency Generation Spectroscopy: Molecular Dynamics Study in Liquid Water" *PCCP* **2018**, *20*, 3040.

(57) Reddy, S. K.; Thiraus, R.; Rudd, B. A. W.; Lin, L.; Adel, T.; Joutsuka, T.; Geiger, F. M.; Allen, H. C.; Morita, A.; Paesani, F.; "Bulk Contributions Modulate the Sum-Frequency Generation Spectra of Water on Model Sea-Spray Aerosols" *Chem.* **2018**, *4*, 1629.

(58) Ohno, P. E.; Chang, H.; Spencer, A. P.; Liu, Y.; Boamah, M. D.; Wang, H.-f.; Geiger, F. M.; "Correction to Beyond the Gouy-Chapman Model with Heterodyne-Detected Second Harmonic Generation" *J. Phys. Chem. Lett.* **2019**, *10*, 5364.

(59) Dreier, L. B.; Bernhard, C.; Gonella, G.; Backus, E. H. G.; Bonn, M.; "Surface Potential of a Planar Charged Lipid–Water Interface. What Do Vibrating Plate Methods, Second Harmonic and Sum Frequency Measure?" *The Journal of Physical Chemistry Letters* **2018**, *9*, 5685.

(60) Rehl, B.; Rashwan, M.; DeWalt-Kerian, E. L.; Jarisz, T. A.; Darlington, A. M.; Hore, D. K.; Gibbs, J. M.; "New Insights into χ(3) Measurements: Comparing Nonresonant Second Harmonic Generation and Resonant Sum Frequency Generation at the Silica/Aqueous Electrolyte Interface" *The Journal of Physical Chemistry C* **2019**, *123*, 10991.

(61) Yan, E. C. Y.; Liu, Y.; Eisenthal, K. B.; "New Method for Determination of Surface Potential of Microscopic Particles by Second Harmonic Generation" *J. Phys. Chem. B* **1998**, *102*, 6331.

(62) Zhao, X.; Ong, S.; Wang, H.; Eisenthal, K. B.; "New method for determination of surface pKa using second harmonic generation" *Chem. Phys. Lett.* **1993**, *214*, 203.

(63) Jacobson, K. H.; Gunsolus, I. L.; Kuech, T. R.; Troiano, J. M.; Melby, E. S.; Lohse, S. E.; Hu, D.; Chrisler, W. B.; Murphy, C. J.; Orr, G.; Geiger, F. M.; Haynes, C. L.; Pedersen, J. A.; "Lipopolysaccharide Density and Structure Govern the Extent and Distance of Nanoparticle Interaction with Actual and Model Bacterial Outer Membranes" *Environ. Sci. Technol.* **2015**, *49*, 10642.

(64) Akesson, A.; Lind, T.; Ehrlich, N.; Stamou, D.; Wacklin, H.; Cardenas, M.; "Composition and structure of mixed phospholipid supported bilayers formed by POPC and DPPC" *Soft Matter* **2012**, *8*, 5658.

(65) Dalstein, L.; Chiang, K.-Y.; Wen, Y.-C.; "Direct Quantification of Water Surface Charge by Phase-Sensitive Second Harmonic Spectroscopy" *J. Phys. Chem. Lett.* **2019**, *10*.

(66) Joutsuka, T.; Morita, A.; "Electrolyte and Temperature Effects on Third-Order Susceptibility in Sum-Frequency Generation Spectroscopy of Aqueous Salt Solutions" *The Journal of Physical Chemistry C* **2018**.

(67) Dalstein, L.; Chiang, K.-Y.; Wen, Y.-C.; "Direct Quantification of Water Surface Charge by Phase-Sensitive Second Harmonic Spectroscopy" *The Journal of Physical Chemistry Letters* **2019**, *10*, 5200.

(68) Wei, X.; Hong, S.-C.; Lvovsky, A. I.; Held, H.; Shen, Y. R.; "Evaluation of Surface vs Bulk Contributions in Sum-Frequency Vibrational Spectroscopy Using Reflection and Transmission Geometries" *The Journal of Physical Chemistry B* **2000**, *104*, 3349.

(69) Yamaguchi, S.; Shiratori, K.; Morita, A.; Tahara, T.; "Electric quadrupole contribution to the nonresonant background of sum frequency generation at air/liquid interfaces" *The Journal of Chemical Physics* **2011**, *134*, 184705.

(70) Lutgebaucks, C.; Gonella, G.; Roke, S.; "Optical label-free and model-free probe of the surface potential of nanoscale and microscopic objects in aqueous solution" *Phys. Rev. B* **2016**, *94*, 195410.

(71) Lütgebaucks, C.; Gonella, G.; Roke, S.; "Optical label-free and model-free probe of the surface potential of nanoscale and microscopic objects in aqueous solution" *Phys. Rev. B: Condens. Matter* **2016**, *94*, 195410.

(72) Shiratori, K.; Yamaguchi, S.; Tahara, T.; Morita, A.; "Computational analysis of the quadrupole contribution in the second-harmonic generation spectroscopy for the water/vapor interface" *J. Chem. Phys.* **2013**, *138*, 064704.

(73) Yamaguchi, S.; Shiratori, K.; Morita, A.; Tahara, T.; "Electric quadrupole contribution to the nonresonant background of sum frequency generation at air/liquid interfaces" *J. Chem. Phys.* **2013**, *134*, 184705.

(74) Higgins, S. R.; Stack, A. G.; Knauss, K. G.; Eggleston, C.; Jordan, G. In *Water-Rock Interactions, Ore Deposits, and Environmental Geochemistry: A Tribute to David A. Crerar*; Hellmann, R. E., Ed.; The Geochemical Society: 2002; Vol. 7.

(75) Mondal, J. A.; Nihonyanagi, S.; Yamaguchi, S.; Tahara, T.; "Three Distinct Water Structures at a Zwitterionic Lipid/Water Interface Revealed by Heterodyne-Detected Vibrational Sum Frequency Generation" *Journal of the American Chemical Society* **2012**, *134*, 7842.

(76) Troiano, J. M.; McGeachy, A. C.; Olenick, L. L.; Fang, D.; Liang, D.; Hong, J.; Kuech, T. R.; Caudill, E. R.; Pedersen, J. A.; Cui, Q.; Geiger, F. M.; "Quantifying the Electrostatics of Polycation–Lipid Bilayer Interactions" *J. Am. Chem. Soc.* **2017**, *139*, 5808.

(77) Brown, K. L.; Conboy, J. C.; "Lipid Flip-Flop in Binary Membranes Composed of Phosphatidylserine and Phosphatidylcholine" *The Journal of Physical Chemistry B* **2013**, *117*, 15041.

(78) Brown, K. L.; Conboy, J. C.; "Electrostatic Induction of Lipid Asymmetry" *J. Am. Chem. Soc.* **2011**, *133*, 8794.

(79) Anglin, T. C.; Cooper, M. P.; Li, H.; Chandler, K.; Conboy, J. C.; "Free Energy and Entropy of Activation for Phospholipid Flip-Flop in Planar Supported Lipid Bilayers" *J. Phys. Chem. B* **2010**, *114*, 1903.

(80) Anglin, T. C.; Conboy, J. C.; "Kinetics and Thermodynamics of Flip-Flop in Binary Phospholipid Membranes Measured by Sum-Frequency Vibrational Spectroscopy" *Biochemistry* **2009**, *48*, 10220.

(81) Anglin, T. C.; Brown, K. L.; Conboy, J. C.; "Phospholipid flip-flop modulated by transmembrane peptides WALP and melittin" *J Struct Biol* **2009**, *168*, 37.

(82) Anglin, T. C.; Liu, J.; Conboy, J. C.; "Facile lipid flip-flop in a phospholipid bilayer induced by gramicidin A measured by sum-frequency vibrational spectroscopy" *Biophys J* **2007**, *92*, L01.

(83) Doğangün, M.; Hang, M. N.; Machesky, J.; McGeachy, A. C.; Dalchand, N.; Hamers, R. J.; Geiger, F. M.; "Evidence for Considerable Metal Cation Concentrations from Lithium Intercalation Compounds in the Nano–Bio Interface Gap" *The Journal of Physical Chemistry C* **2017**, *121*, 27473.

(84) Doğangün, M.; Hang, M. N.; Troiano, J. M.; McGeachy, A. C.; Melby, E. S.; Pedersen, J. A.; Hamers, R. J.; Geiger, F. M.; "Alteration of Membrane Compositional Asymmetry by LiCoO2 Nanosheets" *ACS Nano* **2015**, *9*, 8755.

(85) Troiano, J. M.; Olenick, L. L.; Kuech, T. R.; Melby, E. S.; Hu, D.; Lohse, S. E.; Mensch, A. C.; Dogangun, M.; Vartanian, A. M.; Torelli, M. D.; Ehimiaghe, E.; Walter, S. R.; Fu, L.; Anderton, C. R.; Zhu, Z.; Wang, H.; Orr, G.; Murphy, C. J.; Hamers, R. J.; Pedersen, J. A.; Geiger, F. M.; "Direct Probes of 4 nm Diameter Gold Nanoparticles Interacting with Supported Lipid Bilayers" *The Journal of Physical Chemistry C* **2015**, *119*, 534.

(86) Shapovalov, V. L.; Brezesinksi, G.; "Breakdown of the Gouy-Chapman Model for Highly Charged Langmuir Monolayers: Counterion Size Effect" *J. Phys. Chem. B* **2006**, *110*, 10032.

(87) Olenick, L. L.; Chase, H. M.; Fu, L.; Zhang, Y.; McGeachy, A. C.; Dogangun, M.; Walter, S. R.; Wang, H.-f.; Geiger, F. M.; "Single-component supported lipid bilayers probed using broadband nonlinear optics" *Physical Chemistry Chemical Physics* **2018**, *20*, 3063.

(88) Dogangun, M.; Ohno, P. E.; Liang, D.; McGeachy, A. C.; Be, A. G.; Dalchand, N.; Li, T.; Cui, Q.; Geiger, F. M.; "Hydrogen-Bond Networks near Supported Lipid Bilayers from Vibrational Sum Frequency Generation Experiments and Atomistic Simulations" *J. Phys. Chem. B* **2018**, *122*, 4870.

(89) Gibbs-Davis, J. M.; Kruk, J. J.; Konek, C. T.; Scheidt, K. A.; Geiger, F. M.; "Jammed Acid-Base Chemistry at Interfaces" *J. Am. Chem. Soc.* **2008**, *130*, 15444.

(90) Mifflin, A. L.; Musorrafiti, M. J.; Konek, C. T.; Geiger, F. M.; "Second Harmonic Generation Phase Measurements of Cr(VI) at a Buried Interface" *J. Phys. Chem. B.* **2005**, *109*, 24386.

(91) Mifflin, A. L.; Konek, C. T.; Geiger, F. M.; "Tracking oxytetracyline mobility across environmental interfaces by second harmonic generation" *Journal of Physical Chemistry B* **2006**, *110*, 22577.

(92) Mifflin, A. L.; Gerth, K. A.; Weiss, B. M.; Geiger, F. M.; "Surface studies of chromate binding to fused quartz/water interfaces" *J. Phys. Chem. A* **2003**, *107*, 6212.

(93) Mifflin, A. L.; Gerth, K. A.; Geiger, F. M.; "Kinetics of Chromate Adsorption and Desorption at Fused Quartz/Water Interfaces Studied by Second Harmonic Generation" *J. Phys. Chem. A* **2003**, *107*, 9620.

(94) Al-Abadleh, H. A.; Mifflin, A. L.; Bertin, P. A.; Nguyen, S. T.; Geiger, F. M.; "Control of Carboylic Acid and Ester Groups on Chromium (VI) Binding to Functionalized Fused Silica/Water Interfaces Studied by Second Harmonic Generation" *J. Phys. Chem. B.* **2005**, *109*, 9691.

(95) Al-Abadleh, H. A.; Mifflin, A. L.; Musorrafiti, M. J.; Geiger, F. M.; "Kinetic studies of chromium (VI) binding to carboxylic acid- and methyl ester-functionalized silica/water interfaces important in geochemistry" *Journal of Physical Chemistry B* **2005**, *109*, 16852.

(96) Al-Abadleh, H. A.; Voges, A. B.; Bertin, P. A.; Nguyen; Geiger, F. M.; "Chromium(VI) Binding to Functionalized Silica/Water Interfaces Studied by Nonlinear Optical Spectroscopy" *Journal of the American Chemical Society* **2004**, *126*, 11126.

(97) Konek, C. T.; Illg, K. D.; Al-Abadleh, H. A.; Voges, A. B.; Yin, G.; Musorrafiti, M. J.; Schmidt, C. M.; Geiger, F. M.; "Nonlinear Optical Studies of the Agricultural Antibiotic Morantel Interacting with Silica/Water Interfaces" *Journal of the American Chemical Society* **2005**, *127*, 15771.

(98) Musorrafiti, M. J.; Konek, C. T.; Hayes, P. L.; Geiger, F. M.; "Interaction of Chromium(VI) with the alpha-Aluminum Oxide-Water Interface" *J. Phys. Chem. C* **2008**, *112*, 2032.

(99) Boman, F. C.; Gibbs-Davis, J. M.; Heckman, L. M.; Stepp, B. R.; Nguyen, S. T.; Geiger, F. M.; "DNA at Aqueous/Solid Interfaces: Chirality-Based Detection via Second Harmonic Generation Activity" *Journal of the American Chemical Society* **2009**, *131*, 844.

(100) Troiano, J. M.; Jordan, D. S.; Hull, C. J.; Geiger, F. M.; "Interaction of Cr(III) and Cr(VI) with Hematite Studied by Second Harmonic Generation" *The Journal of Physical Chemistry C* **2013**, *117*, 5164.

(101) Troiano, J. M.; Olenick, L. L.; Keuch, T. R.; Melby, E. S.; Hu, D.; Lohse, S. E.; Mensch, A. C.; Dogangun, M.; Vartanian, A. M.; Torelli, M. D.; Ehimiaghe, E.; Walter, S. R.; Fu, L.; Anderton, C. R.; Zhu, Z.; Wang, H.; Orr, G.; Murphy, C. J.; Hamers, R. J.; Pedersen, J. A.;

Geiger, F. M.; "Direct probes of 4 nm diameter gold nanoparticles interacting with supported lipid bilayers" *J. Phys. Chem. C* **2015**, *119*, 534.

(102) Troiano, J. M.; Kuech, T. R.; Vartanian, A. M.; Torelli, M. D.; Sen, A.; Jacob, L. M.; Hamers, R. J.; Murphy, C. J.; Pedersen, J. A.; Geiger, F. M.; "On Electronic and Charge Interference in Second Harmonic Generation Responses from Gold Metal Nanoparticles at Supported Lipid Bilayers" *The Journal of Physical Chemistry C* **2016**.

(103) Boman, F. C.; Musorrafiti, M. J.; Gibbs, J. M.; Stepp, B. R.; Salazar, A. M.; Nguyen, S. T.; Geiger, F. M.; "DNA Single Strands Tethered to Fused Quartz/Water Interfaces Studied by Second Harmonic Generation" *J. Am. Chem. Soc.* **2005**, *127*, 15368.

(104) Heinz, T. F. *"Second-Order Nonlinear Optical Effects at Surfaces and Interfaces," (Review Chapter) in Nonlinear Surface Electromagnetic Phenomena*; Elsevier: Amsterdam, 1991.

Figure Captions.

Figure 1. Structures of lipids and polycation studied here. A) DOPC, B) DMPC, C) DSPC, D) DMPG, and E) PAH.

Figure 2. Argand diagram demonstrating the phase angle shift effect on the expected SHG response at A) high ionic strength, B) low ionic strength, and C) after low ionic strength following charge reversal. In B) and C), the ionic strength is low and constant (0.01 mM) so that the DC phase angle is constant as indicated by the dashed lines and the $\chi^{(3)}\Phi(0)$ vector is aligned along them.

Figure 3. A) Observed φ_{sig} and normalized E_{sig} as a function of PAH concentration interacting with a supported lipid bilayer prepared from a 9:1 mix of DMPC:DMPG held at a total ionic strength of 0.01 mM NaCl around the point of charge reversal obtained from fitting interference patterns. B) Absolute $\chi^{(2)}$ and $\Phi(0)$ calculated from data presented in Fig. 3A. C) Argand diagrams constructed using the experimental φ_{sig} and E_{sig} values for marks ①, ②, and ③. Please see text for details.

Figure 4. A) Observed φ_{sig} and normalized E_{sig} values and B) $\Phi(0)$ and $\chi^{(2)}$ point estimates obtained for three zwitterionic lipid bilayers and two mixed zwitterionic:negatively charged bilayer in contact with water that had been air-equilibrated overnight (pH 5.8, 0.002 mM ionic strength).

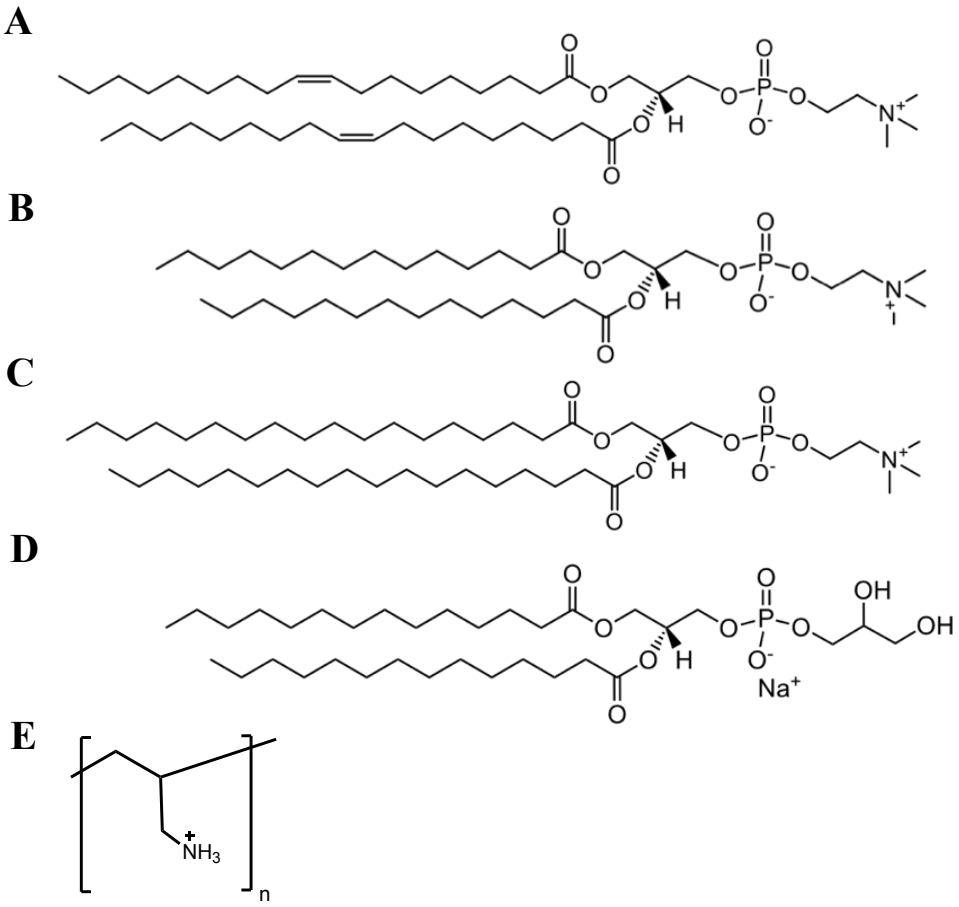

Figure 1.

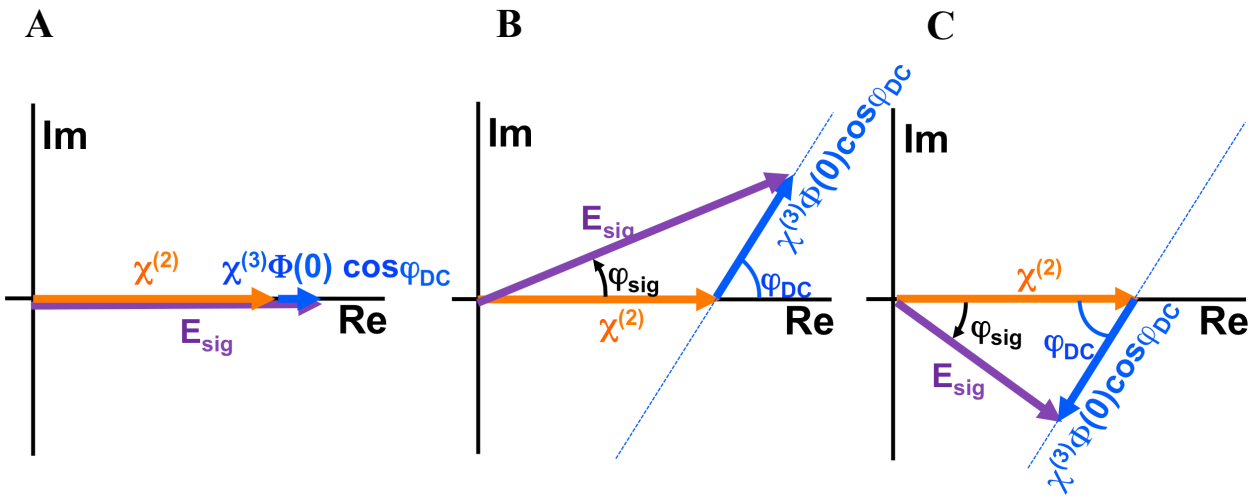
A
Im
Re
$\chi^{(2)}$
$\chi^{(3)}\Phi(0)\cos\varphi_{DC}$
E_{sig}
B
Im
Re
E_{sig}
φ_{sig}
φ_{DC}
$\chi^{(2)}$
$\chi^{(3)}\Phi(0)\cos\varphi_{DC}$
C
Im
Re
$\chi^{(2)}$
φ_{sig}
φ_{DC}
E_{sig}
$\chi^{(3)}\Phi(0)\cos\varphi_{DC}$

Figure 2.

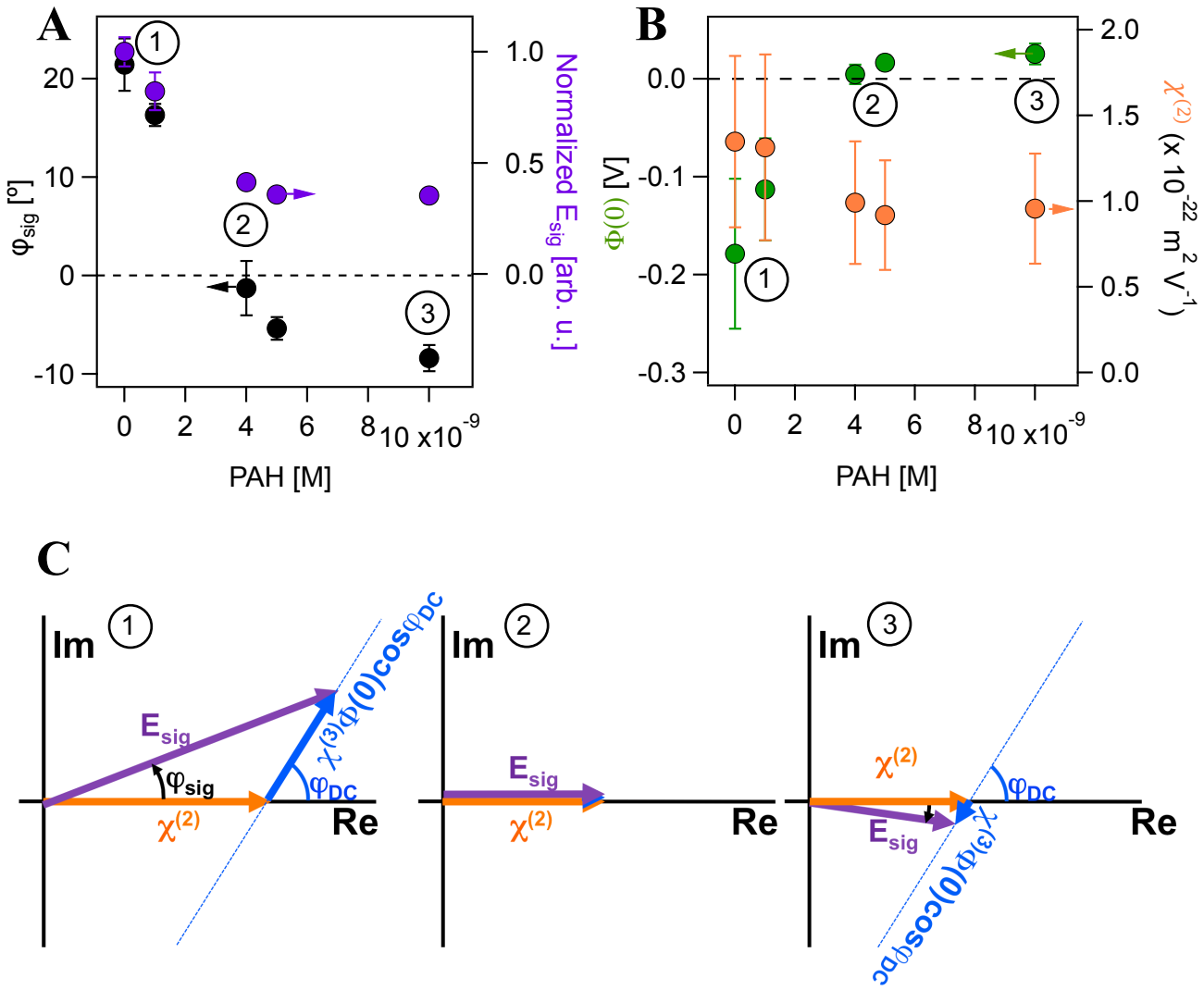
A
B
C
PAH [M]
Normalized E_sig [arb. u.]
φ_sig [°]
Φ(0) [V]
χ(2) (x 10-22 m2 V-1)
10 x10-9
Im
Re
E_sig
φ_sig
χ(2)
φ_DC
χ(3)Φ(0)cosφ_DC
χ(2)Φ(ε)cosφ_DC

Figure 3.

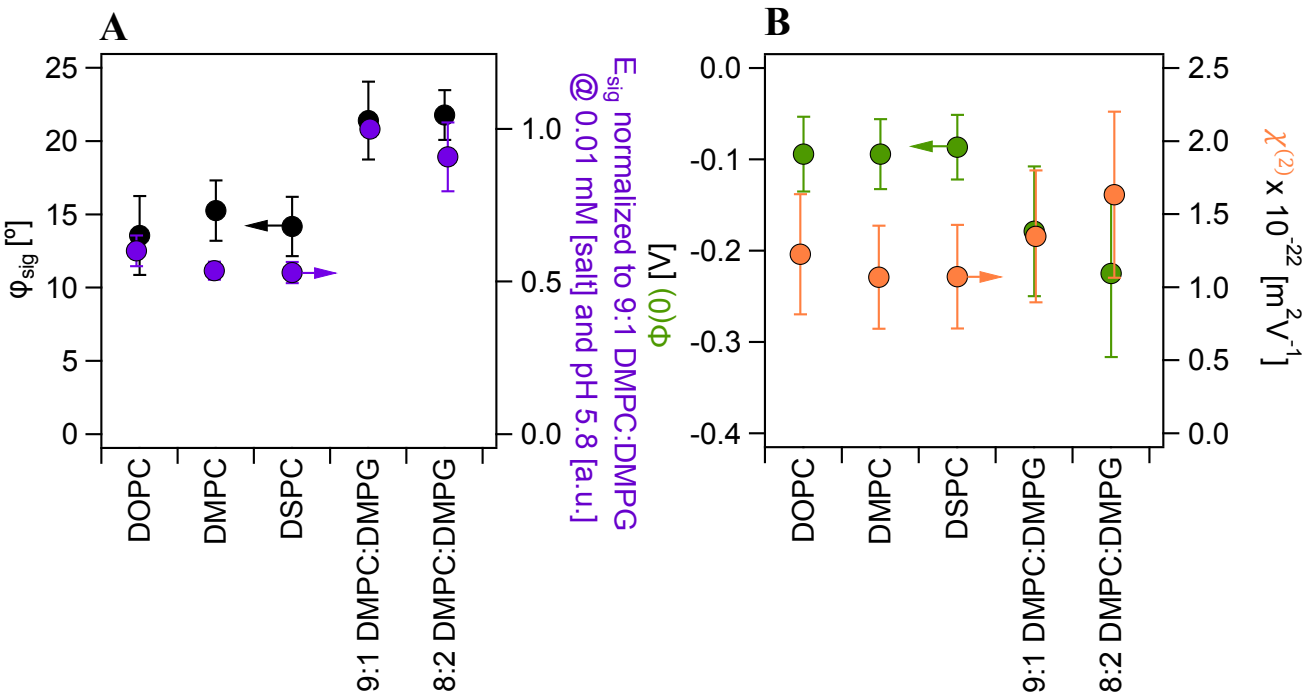
A
B
φ_{sig} [°]
E_{sig} normalized to 9:1 DMPC:DMPG @ 0.01 mM [salt] and pH 5.8 [a.u.]
$\Phi(0)$ [V]
$\chi^{(2)}$ x 10^{-22} [m^2V^{-1}]
DOPC
DMPC
DSPC
9:1 DMPC:DMPG
8:2 DMPC:DMPG

Figure 4.

TOC Graphic

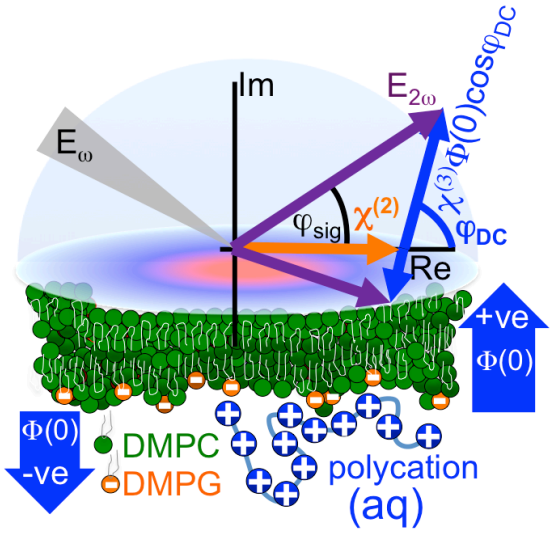
Im
$E_{2\omega}$
E_ω
φ_{sig}
$\chi^{(2)}$
$\chi^{(3)}\Phi(0)\cos\varphi_{DC}$
φ_{DC}
Re
+ve
$\Phi(0)$
$\Phi(0)$
-ve
DMPC
DMPG
polycation
(aq)